

1
2
3
4
5
6
7
8
9
10
11
12
13
14
15
16
17
18
19
20
21
22
23
24
25
26
27
28
29
30
31
32
33
34
35
36
37
38
39
40
41
42
43
44
45
46
47
48
49
50
51
52
53
54
55
56
57
58
59
60
61
62
63
64
65

1 Diatremes act as fluid conduits for Zn-Pb mineralization in the 2 SW Irish Orefield

3 **Holly A. L. Elliott^{1a*}, Thomas M. Gernon¹, Stephen Roberts¹, Adrian J. Boyce² and Chad
4 **Hewson³****

5 *¹ School of Ocean and Earth Science, University of Southampton, National Oceanography
6 Centre Southampton, SO14 3ZH, UK*

7 *²NERC Isotope Facility, Scottish Universities Environmental Research Centre, Rankine Avenue,
8 Scottish Enterprise Technology Park, East Kilbride, G75 0QF, Scotland*

9 *³Teck Resources Limited, Vancouver, Canada*

10 *^a Currently at: Camborne School of Mines, University of Exeter, Penryn Campus, Cornwall,
11 TR10 9FE, UK*

12 **Corresponding author email address: h.elliott@exeter.ac.uk*

14 **ABSTRACT**

15 ‘Irish-type’ mineralization is commonly attributed to fault-controlled mixing of a
16 seawater-derived, sulfur-rich fluid and basement-derived metal-rich fluid. However, maar-
17 diatreme volcanoes discovered in close spatial and temporal association with Zn-Pb
18 mineralization at Stonepark, in the Limerick Basin (SW Ireland) bring a new dimension to
19 established geological models, which may increase the deposit-scale prospectivity in one of the
20 world’s greatest Zn-Pb districts. Stonepark exhibits many incidences of dolomitic black matrix
21 breccias (BMB) with associated Zn-Pb mineralization, the latter typically occurring within 150
22 m of the diatremes. Highly negative $\delta^{34}\text{S}$ pyrite values within country rock-dominated BMBs (-

1
2
3
4 23 12 to -34 ‰) are consistent with sulfide precipitation from bacteriogenic sulfur reduction in
5
6 24 seawater-derived brines. However, $\delta^{34}\text{S}$ values of Zn-Pb sulfides replacing BMBs (-10 to +1 ‰)
7
8
9 25 reflect multiple sulfur sources. Diatreme emplacement both greatly enhanced country rock
10
11 26 fracture permeability, and produced conduits filled with porous volcanoclastic material, that
12
13
14 27 extend down to basement lithologies. Our $\delta^{34}\text{S}$ data suggest that diatremes provide more efficient
15
16 28 fluid pathways for basement-derived fluids. The diatremes introduce another potential sulfur
17
18
19 29 source, and facilitate a greater input of metal-rich basement-derived hydrothermal fluid into the
20
21 30 system compared to other Irish-type deposits such as Navan and Lisheen, evidenced by
22
23
24 31 Stonepark's more positive modal $\delta^{34}\text{S}$ value of -4 ‰. Irish-type deposits are traditionally thought
25
26 32 to form in association with extensional basement faults, and are considered to be unrelated to
27
28
29 33 extensive Carboniferous magmatism. Our results indicate that a direct link exists between
30
31 34 diatreme volcanism and Zn-Pb mineralization at Limerick, prompting a re-evaluation of the
32
33
34 35 traditional 'Irish-type' ore formation model where mineralization is spatially associated with
35
36 36 volcanic pipes.
37

38 INTRODUCTION

39 The Irish Orefield hosts a number of globally important stratabound, carbonate-hosted Zn-Pb
40
41 40 deposits of Viséan age (346.7-330.9 Ma), which exhibit strong spatial and genetic associations
42
43
44 41 with reactivated Caledonian basement faults (Mitchell, 1985; Hitzman & Beaty, 1996; Everett et
45
46
47 42 al., 1999; Hitzman, 1999; Blakeman et al., 2002; Wilkinson et al., 2005a; Hnatyshin et al., 2015;
48
49
50 43 Ashton et al., 2016), and are designated 'Irish-type'. Mineralization in the Limerick region is
51
52
53 44 typically hosted in dolomitized country rock breccias termed 'black matrix breccias' (BMB)
54
55
56 45 (Hitzman et al., 2002; Wilkinson et al., 2005b; Redmond, 2010). The exact origin of these
57
58
59
60
61
62
63
64
65

1
2
3
4 46 deposits remains controversial as they share characteristics of both sedimentary exhalative
5
6 47 (SEDEX; Wilkinson, 2014) and Mississippi Valley-type (MVT) deposits (Bradley & Leach,
7
8
9 48 2003). The 2010 discovery of base-metal mineralization associated with volcanic rocks in SW
10
11 49 Ireland (Blaney et al., 2013; Redmond, 2010) challenged the traditional Irish-type model, which
12
13
14 50 does not recognize a link to volumetrically minor, but regionally extensive Carboniferous
15
16 51 magmatism that extends across Ireland, Scotland and the English Midlands (Woodcock and
17
18
19 52 Strachan, 2000; Holland and Sanders, 2009; Elliott et al., 2015). Field observations at Limerick
20
21 53 (Fig. 1) suggest a close spatial and temporal association between Zn-Pb mineralization and
22
23
24 54 basaltic maar-diatreme volcanism (McCusker and Reed, 2013; Elliott et al., 2015), but the
25
26 55 existence of a direct genetic link is yet to be established.
27
28
29 56

30
31 57 Here, we apply $\delta^{34}\text{S}$ analysis of sulfides from mineralized environments including volcanic
32
33 58 facies and BMBs at Stonepark, Limerick to investigate the relationship between volcanism and
34
35
36 59 ore deposition. Our data indicates that diatreme emplacement strongly influenced mineral deposit
37
38 60 formation at Stonepark. Diatremes, such as those preserved at Stonepark (Elliott et al., 2015),
39
40
41 61 are typically infilled with porous and permeable material (e.g. White and Ross, 2011; Afanasyev
42
43 62 et al., 2014), and are associated with fracture networks and breccia bodies related to their
44
45
46 63 explosive emplacement (Sparks et al., 2006). We propose that the relatively permeable diatremes
47
48 64 served as conduits for mineralizing fluids, forming more efficient fluid pathways from the
49
50
51 65 basement than the extensional fault systems widely observed within the Irish Orefield (e.g.
52
53 66 Silvermines, Navan, Lisheen). Our data also suggest that large quantities of volcanoclastic
54
55
56 67 material within the diatreme provided a third (magmatic) sulfur source.
57
58 68

1
2
3
4 69 *Context and Mineralization*

5
6 70 Maar-diatremes (hereafter, diatremes) are formed during explosive volcanism (cf. Sparks et al.,
7
8 91 2006; White and Ross, 2011). In the Limerick Basin, diatremes form a NE-SW orientated
10
11 72 cluster, closely reflecting the regional Caledonian trend. This suggests that ascending magmas
12
13 73 utilized pre-existing faults (cf. Kurszlaukis and Barnett, 2003; Jelsma et al., 2009).
14
15 74 Phreatomagmatic eruption of these diatremes into a shallow-water graben resulted in the
16
17 75 deposition of >450 m of extra-vent pyroclastic deposits (Knockroe Formation) interbedded with
18
19 76 wackestones and cherts (Elliott et al., 2015). Stratigraphic constraints suggest diatreme
20
21 77 emplacement occurred during the Viséan Stage (346.7–330.9 Ma) (Somerville et al., 1992;
22
23 78 Holland and Sanders, 2009).
24
25
26
27

28
29 79 The Limerick Basin occupies a highly faulted section of the western Irish Midlands (Fig.
30
31 80 1). Here, shallow marine carbonates were deposited during the Lower Carboniferous (Holland
32
33 81 and Sanders, 2009). Typically, it is the Waulsortian Limestone Formation that hosts high
34
35 82 incidences of BMB. Three main types of BMB are recognized at Limerick (Fig. 2), all of which
36
37 83 have a dolomite-rich matrix (≤ 80 wt. %). ‘Country Rock BMB’ (Type C) contains Waulsortian
38
39 84 carbonate clasts, commonly with embayed edges set in a dark, relatively unmineralized matrix
40
41 85 that exhibits limited pyrite replacement (Fig. 2A). ‘Replaced BMB’ (Type R) contains clasts and
42
43 86 matrix completely or predominantly replaced by sphalerite, galena and pyrite (Fig. 2B).
44
45
46
47 87 ‘Polymict BMB’ (Type P) contains a range of clast types including diatreme breccia,
48
49 88 pyroclastics, crystalline igneous and country rock in a poorly-mineralized dolomite matrix (Fig.
50
51 89 2C) intruded by tuffisite dikes. Volcaniclastic material within the breccia occasionally shows
52
53 90 evidence of deformation prior to lithification (Elliott, 2015), indicating that these clasts were still
54
55 91 unconsolidated when they were incorporated into the breccia.
56
57
58
59
60
61
62

1
2
3
4 92 Mineralized or BMB clasts have not yet been observed in the diatreme fill, which has
5
6 93 been dolomitized and subsequently haematitized causing a red coloration. Dolomitization of the
7
8
9 94 diatreme fill starts at ~100-190 meters below sea level (mbsl), coinciding with higher incidences
10
11 95 of BMB in the country rock (Fig. 1). Concentrations of dolomite within the upper diatreme fill
12
13
14 96 range from 0.2 to 0.4 wt.%, increasing to 11-12 wt.% in the middle diatreme (110-190 mbsl) and
15
16 97 22 wt. % at >400 mbsl. Dolomite is a key BMB mineral phase, comprising ≤ 80 wt.% of the
17
18
19 98 breccia matrix. Further, the lower diatreme-fill (>400 mbsl) exhibits the same mineral
20
21 99 assemblage as BMB Type P clasts, comprising dolomite, illite, calcite and quartz, suggesting
22
23
24 100 they experienced similar hydrothermal alteration (Elliott, 2015). The lower diatreme matrix
25
26 101 contains higher concentrations of disseminated sphalerite, pyrite, rutile and galena than the upper
27
28
29 102 and middle diatreme. These observations strongly suggest that diatreme emplacement pre-dated,
30
31 103 or was synchronous with BMB formation and that mineralization post-dated both events.
32

33 104 BMBs are concentrated in fractured country rock adjacent to the diatremes, typically
34
35
36 105 pinching out with distance from the diatreme margins (Fig. 1C). Major and trace element
37
38 106 signatures of juvenile volcanic fragments in the Type P breccias, diatreme fill and Knockroe
39
40
41 107 Formation pyroclastic material are geochemically near-identical (Elliott et al., 2015).
42

43 108

44

45

46 109 *Role of faulting and hydrothermal fluids*

47

48 110 There is some controversy surrounding the relative importance and timing of large-scale
49
50
51 111 extensional basement faults that provided fluid pathways, however there is a general consensus
52
53 112 that the majority of Irish-type deposits were formed by the epigenetic sulfide replacement of
54
55 113 hydrothermal breccias (e.g. Hitzman and Beaty, 1996; Anderson et al., 1998; Hitzman et al.,
56
57
58 114 2002; Wilkinson et al., 2005b; Redmond, 2010). The timing of mineralization at Lisheen and
59
60
61
62
63

1
2
3
4 115 Silvermines have been constrained by Hnatyshin et al., (2015) to 346.6 ± 3.0 Ma and 334.0 ± 6.1
5
6 116 Ma, respectively, and within a similar timeframe to Stonepark.

7
8
9 117 Different BMB types have been recognized in the literature, however, some show
10
11 118 evidence for formation by sedimentary processes within cavities, later overprinted by
12
13
14 119 hydrothermal fluids (e.g. Lee and Wilkinson, 2002). However, typical BMBs are thought to have
15
16 120 formed by hydrothermal fluids that utilized extensional faults, brecciating the carbonate host-
17
18
19 121 rocks (Hitzman and Beaty, 1996; Hitzman et al., 2002). These breccias were later affected by
20
21 122 large-scale sulfide precipitation (Wilkinson et al., 2005b) upon mixing of surface and basement-
22
23
24 123 derived hydrothermal fluids (Banks et al., 2002; Wilkinson et al., 2005a). The surface fluid is
25
26 124 thought to be a lower temperature ($<140^{\circ}\text{C}$) seawater-derived brine, enriched in reduced
27
28
29 125 bacteriogenic sulfur (-25 to -5 per mil, mean -15 per mil; Fallick et al., 2001), which had
30
31 126 evaporated to reach salinities of up to 25 wt% NaCl. The second, higher temperature (200-
32
33 127 280°C) hydrothermal fluid likely contained a high concentration of metals and minor reduced
34
35
36 128 hydrothermal sulfur (0 to 15 per mil, mean 10 per mil; Fallick et al., 2001), leached from
37
38 129 basement rocks (Fallick et al., 2001; Banks et al., 2002).

40 130 41 42 43 131 *Sulfide description and paragenesis*

44
45 132 Sulfide precipitation at Limerick is multi-stage, similar to other deposits in the Irish
46
47
48 133 Orefield (e.g. Hitzman and Beaty, 1996; Hitzman et al., 2002; Wilkinson et al., 2004; Ashton et
49
50 134 al., 2015). Early fine-grained, disseminated pyrite (pre-ore 1) is observed in all environments but
51
52
53 135 can be associated with rounded aggregates of dark sphalerite within BMB horizons (Fig. 2D).
54
55 136 Another void-filling pyrite mineralization stage follows (pre-ore 2), typically precipitated in
56
57
58 137 layers or with a colloform habit (Fig. 2B and 2D). Within the diatreme fill, this stage is
59
60
61
62
63

1
2
3
4 138 represented by massive or coarse-grained pyrite locally replacing juvenile ash, rimming volcanic
5
6
7 139 clasts or is associated with carbonate-filled voids (Fig. 2F).
8

9 140 The subsequent main ore-forming stage is represented differently in each environment.
10
11 141 Unfortunately, sphalerite and galena crystals within the lower diatreme are too small to perform
12
13
14 142 sulfur isotope analysis, but have been identified and imaged by Scanning Electron Microscope
15
16 143 (SEM) (Fig. 2G). These minerals appear to co-precipitate as anhedral masses predominantly
17
18
19 144 replacing volcanic lapilli or earlier pyrite. Earlier pyrite within BMB samples are brecciated or
20
21 145 replaced by ore minerals at this stage (Fig. 2B and 2C). Within Type R BMB, galena is typically
22
23
24 146 observed as large anhedral crystals and sphalerite as creamy yellow-brown anhedral
25
26 147 intergranular masses, often associated with carbonate filling voids (Fig. 2B). A similar
27
28
29 148 assemblage is observed within the Waulsortian Limestone environment, as veins, replacing
30
31 149 crackle breccias or sediment infilling voids. Sphalerite is typically found at the edge of veins or
32
33
34 150 rimming clasts in breccias, and is occasionally layered, whereas anhedral galena and carbonate
35
36 151 fill the voids (Fig. 2C and 2E). Pure sphalerite veins within the limestone consist of elongate
37
38
39 152 brown crystals. Sphalerite and galena are sparse within Type P BMB samples, but can replace
40
41 153 the matrix and earlier layered or colloform pyrite (Fig. 2D).
42

43 154 Post-ore fine-grained veins of pyrite intrude, brecciate and in some cases replace earlier
44
45
46 155 stages of mineralization (Fig. 2B and 2C). This is observed in all sampled environments except
47
48 156 the volcanic material, in which sphalerite and galena are the latest mineralization stages
49
50
51 157 identified.
52

53 158

54
55 159 **ANALYTICAL TECHNIQUES**
56
57
58
59
60
61
62

1
2
3
4 160 Sulfides (pyrite, sphalerite and galena) from BMBs, sedimentary rocks, intrusions,
5
6
7 161 diatremes and veins were separated from gangue by crushing and picking or micro drill
8
9 162 extraction, and analyzed for sulfur isotopes following the approach used by Robinson and
10
11 163 Kusakabe (1975). Samples of fine-grained sulfides and those exhibiting intergrown sulfide
12
13
14 164 textures were prepared as polished blocks and combusted by in-situ laser analysis (Wagner et al.,
15
16 165 2002). The laser spot size was ~100 μm , significantly smaller than the scale of intergrowths,
17
18
19 166 which typically range from 400-6000 μm . Reproducibility based on repeat analysis of internal
20
21 167 and international standards was $\sim \pm 0.3$ ‰ for both methods. All data are reported in $\delta^{34}\text{S}$ notation
22
23
24 168 as per mil (‰) variations from the Vienna Canyon Diablo Troilite (V-CDT).
25
26
27
28

29 170 **SULFUR ISOTOPE RESULTS**

30
31 171 The Waulsortian Limestone Formation hosts the diatremes, BMB and also contains
32
33
34 172 pyrite-carbonate filled veins and breccias. Limestone-hosted sulfides (pyrite, sphalerite and
35
36 173 galena – see Supplementary Table A1) consist of pre-ore stage 1, stage 2 and ore stage minerals
37
38
39 174 that returned predominantly negative $\delta^{34}\text{S}$ values (-45 to -1 ‰), with a mean of -10.9 ‰. Only
40
41 175 three samples out of the 16 analyzed, show fine-scale inhomogeneity, displaying values up to
42
43
44 176 +12 ‰ (Fig. 3A). Ore stage sulfides display a more positive mean $\delta^{34}\text{S}$ value of -7.5 ‰
45
46 177 compared to pre-ore stages (-17 to -14 ‰).
47

48 178 Type C BMBs contain pre-ore stage pyrite with negative $\delta^{34}\text{S}$ values (-34 to -13 ‰; Fig.
49
50
51 179 3B, Supplementary Table A2). In contrast, >70 % of Type R BMB $\delta^{34}\text{S}$ values (pyrite, sphalerite
52
53 180 and galena) lie in the range -10 to +1 ‰ (mode -4 ‰). Pre-ore stage 2 sulfides (mean -7‰) and
54
55
56 181 ore stage sulfides (mean -5‰) display similar ranges of $\delta^{34}\text{S}$ values. However, pre-ore stage 1
57
58 182 sulfides display more negative $\delta^{34}\text{S}$ values (mean -20 ‰). Type P BMBs are variably
59
60
61
62
63

1
2
3
4 183 mineralized with pyrite and minor sphalerite and galena, reflected in the wide distribution of $\delta^{34}\text{S}$
5
6 184 values (-44 to +10 ‰, Fig. 3B and Supplementary Table A2). Compared to the other BMB
7
8
9 185 environments, Type P ore stage sulfides exhibit more positive $\delta^{34}\text{S}$ values (mean 6‰).
10

11 Sulfides (predominantly pyrite) from volcanic rocks exhibit a more restricted range of
12
13
14 187 $\delta^{34}\text{S}$ values, largely between -10 and +10 ‰ (Fig. 3C). Due to their disseminated nature in the
15
16 188 diatreme fill, ore stage sulfides were only able to be sampled from intrusions, which displayed a
17
18
19 189 mean $\delta^{34}\text{S}$ value of 5.5 ‰. Pre-ore stage 1 sulfide minerals within diatreme and intrusion
20
21 190 samples exhibit more negative $\delta^{34}\text{S}$ values (mean -4 and -7 ‰ respectively) than pre-ore stage 2,
22
23
24 191 which typically show more positive $\delta^{34}\text{S}$ values (mean 2 and 3 ‰ respectively).
25
26 192

27 28 29 193 *Comparison with other deposits in the Irish Orefield* 30

31 194 Sulfides at Silvermines show a bimodal $\delta^{34}\text{S}$ distribution with modes at -21 and -36 ‰
32
33 195 (Fig. 3E). In contrast, minerals from Lisheen show a unimodal $\delta^{34}\text{S}$ distribution with a mode of -
34
35
36 196 10 ‰ (Fig. 3F). Our data from Stonepark (Fig. 3D) have a distinctly more positive distribution
37
38 197 with a mode of -4 ‰ (Supplementary Table A2) compared to the other two deposits. A highly
39
40
41 198 negative pyrite peak is common to all deposits, visible between -40 to -35 ‰ (Fig. 3).
42

43 199 Sulfides adjacent to faults at Navan and Lisheen typically exhibit more positive $\delta^{34}\text{S}$
44
45
46 200 values (Blakeman et al., 2002; Wilkinson et al., 2005b), suggesting they accommodated
47
48 201 basement-derived fluids (Blakeman et al., 2002; Wilkinson et al., 2005b). To some extent this
49
50
51 202 relationship is observed at Limerick, where positive $\delta^{34}\text{S}$ values of sphalerite and galena are
52
53 203 solely observed proximal to the diatremes (<116 m). However, negative $\delta^{34}\text{S}$ values of these
54
55 204 sulfides are observed at all distances from the diatremes, up to 410 m (Fig. 1B and C).
56
57
58
59
60
61
62

1
2
3
4
5
6
7
8
9
10
11
12
13
14
15
16
17
18
19
20
21
22
23
24
25
26
27
28
29
30
31
32
33
34
35
36
37
38
39
40
41
42
43
44
45
46
47
48
49
50
51
52
53
54
55
56
57
58
59
60
61
62
63
64
65

205 Sulfur isotope data for the adjacent Pallas Green deposit (currently owned by Glencore
206 PLC) are sparse, but those available indicate a similarly positive value (~+10 ‰, Wilkinson and
207 Redmond, 2010). A number of volcanic centers have also been identified at Pallas Green, in
208 addition to many dikes, sills and intrusive breccia plugs (Tyler, 2007), with the latter likely to be
209 diatremes. Tyler (2007) also describes breccia dikes containing <30 % igneous clasts,
210 comparable with Type P BMBs described herein, which are often associated with ore-grade
211 mineralization.

DISCUSSION & CONCLUSIONS

214 Grades of Zn and Pb mineralization are high within BMB horizons proximal to the
215 diatremes (≤ 27 wt.% - see Supplementary Table A3), and reduce significantly with distance from
216 the diatreme margins (Fig. 5). This pattern supports the hypothesis that basement-derived metal-
217 rich fluids preferentially utilized the diatremes. Anomalously high Zn concentrations (>20 wt.%)
218 occur at shallower depths adjacent to diatremes in the northwest (Fig. 4C), compared to the
219 southeast (Fig. 4D). Lead concentrations show a similar pattern, displaying <30 wt.% at
220 shallower depths surrounding the northern diatreme-related boreholes (Fig. 4A), however
221 comparable concentrations to the south are observed at 350 m (Fig. 4B). This could be related to
222 the thick composite intrusions observed within diatreme 19 (Fig. 1B and C) acting as a barrier,
223 and focusing fluids in to the surrounding country rock at greater depths to the southwest.

224 Negative $\delta^{34}\text{S}$ values within Type C BMBs are consistent with a bacteriogenic sulfur
225 origin, most likely precipitated from seawater-derived brines. The light sulfur isotopes and lack
226 of ore stage minerals support the hypothesis that metal-rich basement-derived fluids never
227 reached these breccias. In contrast, Type R BMBs show evidence for a shift to more positive

1
2
3
4 228 values, which could be explained by mixing of two fluids, resulting in extensive sulfide
5
6 229 precipitation (Fig. 5B). Early pre-ore stage 1 sulfides display highly negative $\delta^{34}\text{S}$ values,
7
8
9 230 indicating they precipitated from seawater-derived brines. The introduction of metal-rich,
10
11 231 basement-derived fluids containing heavier sulfur isotopes, resulted in more positive isotopic
12
13
14 232 signatures in the later pre-ore stage 2 and ore-stage sulfides.

15
16 233 Type P BMB sulfides exhibit the widest range of $\delta^{34}\text{S}$ values, consistent with
17
18 234 bacteriogenic sulfate reduction (-45 ‰) and more positive sulfur leached from basement rocks
19
20
21 235 (+10 ‰). Heavier sulfur isotopes may also have been leached from the large volumes of
22
23 236 diatreme, intrusion and Knockroe-related material hosted in these breccias, with means between -
24
25
26 237 2.1 and +3.8 ‰ (see Supplementary Table A2). Country rock-hosted sulfides exhibit
27
28 238 predominantly negative $\delta^{34}\text{S}$ values (see Fig. 3A). These data suggest that seawater-derived
29
30
31 239 fluids utilized both fractured country rock and diatreme pathways, whereas basement-derived
32
33 240 fluids were restricted to the diatremes and subsequently formed Type P BMBs (Fig. 5B). Fluid
34
35
36 241 mixing in Type R breccias led to extensive sulfide precipitation.

37
38 242 It is well established that diatreme-filling deposits have high initial porosity and
39
40
41 243 permeability (Sparks et al., 2006; Stripp et al., 2006), allowing enhanced hydrothermal fluid flow
42
43 244 (Afanasyev et al., 2014). Further, diatreme-forming eruptions produce radial fracture networks
44
45
46 245 (cf. Barnett and Lorig, 2007), allowing fluid flow in and out of the diatremes. The localization of
47
48 246 BMB adjacent to, and radiating out from the diatreme margins (Fig. 1B and C), most likely
49
50
51 247 reflects exploitation by fluids of fracture networks associated with diatreme emplacement. High
52
53 248 Zn and Pb grades (<22 and 7.5 wt.% respectively) are also observed <50 m from the diatremes,
54
55 249 and reducing significantly with distance from the diatreme margins (Fig. 4).
56
57
58
59
60
61
62

1
2
3
4
5
6
7
8
9
10
11
12
13
14
15
16
17
18
19
20
21
22
23
24
25
26
27
28
29
30
31
32
33
34
35
36
37
38
39
40
41
42
43
44
45
46
47
48
49
50
51
52
53
54
55
56
57
58
59
60
61
62
63
64
65

250 Hydrothermal components increase in importance during the later stages of Irish-type ore
251 formation (e.g. Lisheen; Wilkinson et al., 2005b). The Stonepark deposit exhibits a more positive
252 sulfur isotope signature in later sulfide precipitation stages compared to other Irish Orefield
253 deposits. We attribute this to enhanced hydrothermal fluid flux from the basement, via 1-2 km
254 deep diatremes, which would increase the amount of hydrothermal sulfur relative to
255 bacteriogenic sulfur in the mineralizing system. In summary, the evidence for enhanced fluid
256 flow from the basement via diatremes is as follows: (1) dolomite, a key BMB mineral, overprints
257 the lower diatreme fill; (2) the occurrence of mineralization within the lower diatremes; (3) high
258 Zn-Pb mineralization grades proximal to diatreme margins (Fig. 4); and (4) the more positive
259 sulfur isotope signatures observed in the Stonepark deposit (Fig. 3C). The latter is enhanced by
260 the leaching of a third magmatic sulfur source (mean -0.4 ‰, see Supplementary Table A1
261 ‘Intrusion (original)’ from basaltic glass-rich pyroclastic diatreme-fill (estimated minimum
262 volume for a given vent $\sim 5 - 7.5 \times 10^6 \text{ m}^3$; Elliott et al., 2015) during hydrothermal alteration (cf.
263 Afansyev et al., 2014).

264 The timing of mineralization in the Irish Orefield (Chadian to Arundian; Hitzman and
265 Beatty, 1996; Anderson et al., 1998; Reed and Wallace, 2004; Ashton et al., 2015) overlaps with
266 extensive magmatic and volcanic activity, including that in the Limerick Basin (Somerville et al.,
267 1992; Elliott et al., 2015; Hnatyshin et al., 2015; Wilkinson and Hitzman, 2015). Textures such
268 as plastic deformation of diatreme-derived material within BMB Type P indicates that BMB
269 formation occurred during the waning stages of diatreme activity. Therefore, a close temporal
270 association between volcanism, hydrothermal activity and mineralization exists at Stonepark, and
271 raises the interesting possibility that volcanism is a key process in the localization of Zn-Pb
272 mineralization. The temporal associations at Limerick are consistent with a scenario in which

1
2
3
4
5
6
7
8
9
10
11
12
13
14
15
16
17
18
19
20
21
22
23
24
25
26
27
28
29
30
31
32
33
34
35
36
37
38
39
40
41
42
43
44
45
46
47
48
49
50
51
52
53
54
55
56
57
58
59
60
61
62
63
64
65

273 magmatism elevated heat flow and hydrothermal circulation in the Carboniferous Irish Orefield
274 (Praeg, 2004; Wilson et al., 2004; Davidheiser-Kroll et al., 2014; Hnatyshin et al., 2015;
275 Wilkinson and Hitzman, 2015).

276 This study has implications for the origin of diatreme-related mineralization in other
277 regions, for example gold deposits such as those of Kelian, Indonesia and Cripple Creek, USA
278 (Davies et al., 2008). Our results suggest that diatreme breccias can focus metal-rich
279 hydrothermal fluids, facilitating epithermal metal deposit formation. The direct link between
280 volcanic activity and Zn-Pb mineralization at Limerick prompts re-evaluation of the traditional
281 ‘Irish-type’ model for ore formation in regions where mineralization is spatially associated with
282 magmatism and volcanic pipes.

284 ACKNOWLEDGMENTS

285 The authors would like to thank Teck Ireland Ltd for supporting this study and Group Eleven
286 Resources for their cooperation. We acknowledge and thank Dr Jon Neades for creating the 3D
287 model portrayed in Figure 4. Funding for isotope analysis was obtained from the Natural
288 Environment Research Council (IP-1397-1113). We would also like to thank the expert staff at
289 the SUERC isotope facility in East Kilbride.

291 REFERENCES CITED

292 Afanasyev, A. A., Melnik, O., Porritt, L., Schumacher, J. C. and Sparks, R. S. J., 2014, Hydrothermal alteration of
293 kimberlite by convective flows of external water: Contributions to Mineralogy and Petrology, v. 168, p. 1038-1055.
294 Anderson, I.K., Ashton, J.H., Boyce, A.J., Fallick, A.E. and Russell, M.J., 1998, Ore depositional processes in the
295 Navan Zn-Pb deposit, Ireland: Economic Geology, v. 93, p. 535-563.
296 Ashton, J. H., Blakeman, R. J., Geraghty, J. F., Beach, A., Collier, D., Phicox, M. E., Boyce, A. J. and Wilkinson, J.

1
2
3
4
5 297 J., 2015, The giant Navan carbonate-hosted Zn-Pb deposit – a review, in Archibald, S. and Piercey, S., eds., Current
6 298 perspectives on zinc deposits: Dublin, Irish Association for Economic Geology, p. 85-122.
7
8
9 299 Banks, D. A., Boyce, A. J. and Samson, I. M., 2002, Constraints on the origins of fluids forming Irish Zn-Pb-Ba
10 300 deposits: Evidence from the composition of fluid inclusions: *Economic Geology*, v. 97, p. 471–480.
11
12
13 301 Barnett, W. and Lorig, L., 2007, A model for stress-controlled pipe growth: *Journal of Volcanology and Geothermal*
14 302 *Research*, v. 159, p. 108–125.
15
16
17 303 Blakeman, R. J., Ashton, J. H., Boyce, A. J., Fallick, Anthony, E. and Russell, M. J., 2002, Timing of interplay
18 304 between hydrothermal and surface fluids in the Navan Zn + Pb orebody, Ireland: evidence from metal distribution
19 305 trends, mineral textures, and δS^{34} analyses: *Economic Geology*, v. 97, p. 73–91.
20
21
22 306 Blaney, D., Tennant, S. and Tyler, P., 2013, Geology, alteration and mineralization of the Pallas Green block,
23 307 Country Limerick, Ireland, in Kelly, J. G., Andrew, C. J., Ashton, J. H., Boland, M. B., Earls, G., Fusciardi, L. and
24 308 Stanley, G., ed., *Europe’s major base metal deposits*: Dublin, Irish Association for Economic Geology, p. 533-544.
25
26
27
28 309 Davidheiser-Kroll, B., Stuart, F. M. and Boyce, A. J., 2014, Mantle heat drives hydrothermal fluids responsible for
29 310 carbonate-hosted base metal deposits: evidence from $3He/4He$ of ore fluids in the Irish Pb-Zn ore district:
30
31 311 *Mineralium Deposita*, v. 49, p. 547–553.
32
33
34 312 Davies, A. G. S., Cooke, D. R., Gemmell, J. B. and Simpson, K. A., 2008, Diatreme breccias at the Kelian gold
35 313 mine, Kalimantan, Indonesia: Precursors to epithermal gold mineralization: *Economic Geology*, v. 103, p. 689-716
36
37
38 314 Elliott, H. A. L., 2015, Pb-Zn mineralisation within the Limerick Basin (SW Ireland): A role for volcanism? PhD
39 315 thesis, Southampton, UK, University of Southampton.
40
41
42 316 Elliott, H. A. L., Gernon, T. M., Roberts, S. and Hewson, C., 2015, Basaltic maar-diatreme volcanism in the Lower
43 317 Carboniferous of the Limerick Basin (SW Ireland): *Bulletin of Volcanology*, v. 77, p. 37-59.
44
45
46 318 Everett, C. E., Wilkinson, J. J. and Rye, D. M., 1999, Fracture-controlled fluid flow in the Lower Palaeozoic
47 319 basement rocks of Ireland: implications for the genesis of Irish-type Zn-Pb deposits, in K. J. W. McCaffrey, L.
48 320 Lonergan and J. J. Wilkinson, ed., *Fractures, fluid flow and mineralization*: London, Geological Society, v. 155, p.
49 321 247-276.
50
51
52
53 322 Fallick, A. E., Ashton, J. H., Boyce, A. J., Ellam, R. M. and Russel, M. J., 2001, Bacteria were responsible for the
54 323 magnitude of the world-class hydrothermal base-metal orebody at Navan, Ireland: *Economic Geology*, v. 96, p. 883-
55 324 888
56
57
58 325 Hitzman, M. W. and Beaty, D. W., 1996, *The Irish Zn-Pb-(Ba) Orefield*: Society of Economic Geologists Special
59 326 Publication no. 4, p. 112–143.
60
61
62
63
64
65

- 1
2
3
4
5 327 Hitzman, M. W., Redmond, P. B. and Beaty, D. W., 2002, The carbonate-hosted Lisheen Zn-Pb-Ag deposit, County
6 328 Tipperary, Ireland: *Economic Geology*, v. 97, p. 1627– 1655.
7
8
9 329 Hitzman, M. W., 1999, Extensional faults that localize Irish syndiagenetic Zn-Pb deposits and their later
10 330 compressional fate, in K. McCaffery, L. Lonergan, and J. Wilkinson, ed. *Fractures, Fluid Flow and Mineralization*:
11 331 London, Geological Society, Special Publications v. 155, p. 233-245.
12
13
14 332 Hnatyshin, D., Creaser, R. A., Wilkinson, J. J. and Gleeson, S. A., 2015, Re-Os dating of pyrite confirms an early
15 333 diagenetic onset and extended duration of mineralization in the Irish Zn-Pb ore field: *Geology*, v. 43, p. 143-146.
16
17
18 334 Holland, C. H. and Sanders, I. S., 2009, *The Geology of Ireland*, 2nd .ed: Dunedin Academic Press.
19
20
21 335 Jelsma, H., Barnett, W., Richards, S. and Lister, G., 2009, Tectonic setting of kimberlites: *Lithos*, v. 112S, p. 155–
22 336 165.
23
24
25 337 Kurszlauskis, S. and Barnett, W., 2003, Volcanological and structural aspects of the Venetia kimberlite cluster - as
26 338 case study of South African kimberlite maar-diatreme volcanoes: *South African Journal of Geology*, v. 106, p. 145–
27 339 172.
28
29
30 340 Lee, M. J. and Wilkinson, J. J., 2002, Cementation, hydrothermal alteration, and Zn-Pb mineralization of carbonate
31 341 breccias in the Irish Midlands: textural evidence from the Coleen Zone, near Silvermines, County Tipperary:
32 342 *Economic Geology*, v. 97, p. 653-662.
33
34
35
36 343 McCusker, J. and Reed, C., 2013, The role of intrusions in the formation of Irish-type mineralisation: *Mineralium*
37 344 *Deposita*, v. 48, p. 687–695.
38
39
40 345 Mitchell, A. H. G., 1985, Mineral deposits related to tectonic events accompanying arc-continent collision:
41 346 *Transactions of the Institution of Mining and Metallurgy*, v. 94, p. 115-125.
42
43
44 347 Praeg, D., 2004, Diachronous Variscan late-orogenic collapse in response to multiple detachments: a view from the
45 348 Internides in France to the foreland in the Irish Sea, in M. Wilson, E. R. Neumann, G. R. Davies, M. J. Timmerman,
46 349 M. Heeremans and B. T. Larsen, ed., *Permo-Carboniferous Magmatism and Rifting in Europe*: Geological Society
47 349 of London, v. 223, p. 89 – 138.
48
49
50
51 351 Redmond, P. B., 2010, The Limerick Basin: An important emerging subdistrict of the Irish Zn-Pb orefield: *Society*
52 352 *of Economic Geologists Newsletter*, v. 82, p. 21–25.
53
54
55 353 Reed, C. P. and Wallace, M. W., 2004, Zn-Pb mineralisation in the Silvermines district, Ireland: a product of burial
56 354 diagenesis: *Mineralium Deposita*, v. 39, p. 87–102.
57
58
59 355 Robinson, B. W. and Kusakabe, M., 1975, Quantitative preparation of sulfur dioxide, for $^{34}\text{S}/^{32}\text{S}$ analyses, from
60
61
62
63
64
65

- 1
2
3
4
5 356 sulfides by combustion with cuprous oxide: *Analytical Chemistry*, v. 47, p. 1179–1181.
6
7 357 Somerville, I. D., Strogon, P. and Jones, G. L., 1992, Biostratigraphy of Dinantian limestones and associated
8
9 358 volcanic rocks in the Limerick Syncline, Ireland: *Geological Journal*, v. 27, p. 201–220.
10
11 359 Sparks, R. S. J., Baker, L., Brown, R. J., 2006, Dynamical constraints on kimberlite volcanism: *Journal of*
12
13 360 *Volcanology and Geothermal Research*, v. 155, p. 18-48.
14
15 361 Stripp, G. R., Field, M., Schumacher, J. C., Sparks, R. S. J. and Cressy, G., 2006, Post- emplacement
16
17 362 serpentinization and related hydrothermal metamorphism in a kimberlite from Venetia, South Africa: *Journal of*
18
19 363 *Metamorphic Geology*, v. 24, p. 515–534.
20
21 364 Tyler, P. A., 2007, An evaluation of potential, Pallas Green Property, Co. Limerick and Tipperary, Ireland:
22
23 365 Unpublished report prepared for Minco Plc, Durham, England.
24
25 366 Wagner, T., Boyce, A.J. and Fallick, A.E., 2002, Laser combustion analysis of $\delta^{34}\text{S}$ of sulfosalt minerals:
26
27 367 determination of the fractionation systematics and some crystal-chemical considerations: *Geochimica*
28
29 368 *Cosmochimica Acta*, v. 66, p. 2855-2863.
30
31 369 White, J. D. L. and Ross, P.-S., 2011, Maar-diatreme volcanoes: a review: *Journal of Volcanology and Geothermal*
32
33 370 *Research*, v. 201, p. 1–29.
34
35 371 Wilkinson, J. J., Everett, C. E., Boyce, A. J., Gleeson, S. A. and Rye, D. M., 2005a, Intracratonic crustal seawater
36
37 372 circulation and the genesis of subseafloor zinc-lead mineralization in the Irish orefield: *Geology*, v. 33, p. 805–808.
38
39 373 Wilkinson, J. J., Eyre, S. L. and Boyce, A. J., 2005b, Ore-forming processes in Irish- Type carbonate-hosted Zn-Pb
40
41 374 deposits: Evidence from mineralogy, chemistry, and isotopic composition of sulfides at the Lisheen Mine: *Economic*
42
43 375 *Geology*, v. 100, p. 63–86.
44
45 376 Wilkinson, J. J. and Redmond, P. B., 2010, Irish Zn-Pb: New insights, new discoveries: IAGOD Symposium
46
47 377 conference presentation, Adelaide, Australia.
48
49 378 Wilkinson, J. J., 2014, Sediment-hosted zinc-lead mineralization: Processes and Perspectives, in H. D. Holland and
50
51 379 K. K. Turekian, ed., *Geochemistry of Mineral Deposits*: Oxford, Elsevier, p. 219-249.
52
53 380 Wilkinson, J. J. and Hitzman, M. W., 2015, The Irish Zn-Pb Orefield: The view from 2014, in S. M. Archibald and
54
55 381 S. J. Piercey, ed., *Current perspective on zinc deposits*: Dublin, Irish Association for Economic Geology, p. 59-72.
56
57 382 Wilson, B., Neumann, E. R., Davies, G. R., Timmerman, M. J., Heeremans, M. and Larsen, B. T., 2004, Permo-
58
59 383 Carboniferous Magmatism and Rifting in Europe: London, Special Publication, Geological Society of London.
60
61
62
63
64
65

1
2
3
4
5
6
7
8
9
10
11
12
13
14
15
16
17
18
19
20
21
22
23
24
25
26
27
28
29
30
31
32
33
34
35
36
37
38
39
40
41
42
43
44
45
46
47
48
49
50
51
52
53
54
55
56
57
58
59
60
61
62
63
64
65

384 Woodcock, N. H. and Strachan, R., 2000, Geological history of Britain and Ireland: Oxford, Blackwell Science.

385

386 **FIGURE CAPTIONS**

387 Fig. 1. A: Summary geologic map of the study area outlined with a white line, showing inferred
388 diatreme outlines (resolved by drill-core and magnetic surveys) and boreholes intersecting
389 diatremes. Inset map of Ireland shows the location of Limerick. B: South-west to north-east cross
390 section. C: West to east cross section (see A for locations) showing diatremes and adjacent
391 BMBs. Dotted lines on diatremes indicate upper extent of dolomitization and subsequent
392 hematization overprinting basal parts of diatremes. Y-axis depicts height relative to sea level.

393

394 Fig. 2. A: Summary of the mineralogy and relative importance of each stage of volcanism,
395 dolomitization and mineralization within the studied categories. Note that Dol: dolomite, Ap:
396 apatite, It: illite, Pyr: pyrite, Sph: sphalerite, Gal: galena, Carb: carbonate. B: Sample 6476 –
397 Replacement of BMB (Type R) by layered pre-ore stage 2 pyrite and ore stage minerals
398 brecciated by post-ore fine-grained pyrite. C: Sample 6508 – Replacement of limestone breccia
399 by the same mineral assemblage seen in B. D: Sample 6470 – Polymict breccia (Type P)
400 replaced by layered and colloform stage 2 pyrite, later replaced by ore stage spherules of
401 sphalerite. E: Sample 6500 – Ore stage vein of sphalerite, galena and carbonate cross-cutting
402 Waulsortian Limestone. F: Sample 6496 – Pyrite replaced by sphalerite rimming clasts in
403 diatreme fill. G: Sample S17 – SEM image of sphalerite replacing matrix of diatreme clast. H:
404 Country rock breccias (Type C) - Weakly mineralized with minor pyrite and Waulsortian
405 Limestone clasts displaying embayed edges and often jigsaw or float textures (borehole TC-

1
2
3
4
5
6
7
8
9
10
11
12
13
14
15
16
17
18
19
20
21
22
23
24
25
26
27
28
29
30
31
32
33
34
35
36
37
38
39
40
41
42
43
44
45
46
47
48
49
50
51
52
53
54
55
56
57
58
59
60
61
62
63
64
65

406 2638-036, 223.1 mbsl). I: Polymict breccias (Type P) - diatreme clasts and matrix partially
407 replaced by pyrite (borehole TC-2638-047, 0.6 mbsl).

408
409 Fig. 3. Histograms of sulfur isotope results (raw data available in Supplementary Table A1). A:
410 Data categorized by environments: BMB, limestone and volcanic rock-hosted sulfides. B: BMB
411 data categorized by type. Type R contain high concentrations of sulfides; Type P moderate
412 concentrations, predominantly pyrite; and Type C are typically unmineralized. C: Volcanic-
413 hosted sulfide data generalized in Figure 3A, is here categorized by host-rock (diatreme fill,
414 intrusions or extra-crater deposits of the Knockroe Formation). D: Sulfur isotope results
415 categorized by mineral type from all environments. For comparison, sulfur isotope data from (E)
416 Silvermines (Boyce et al., 2003) and (F) Lisheen (Wilkinson et al., 2005b) are shown categorized
417 by mineral type.

418
419 Fig. 4. 3D box models displaying variations in concentration of lead and zinc (ppm), showing
420 plan sections through the model at varying depths within the northeast section of the Limerick
421 license area. Grey lines show depths within boreholes where assay Zn and Pb concentrations
422 have been measured (see Supplementary Table A3). The model was created by extrapolating
423 these values in all directions. Dotted blue lines show traces of diatreme-related boreholes
424 identified by the number above, and depth is recorded as metres below sea level (mbsl). 3D box
425 models display lead concentrations with plan sections at 100 mbsl (A) and 350 mbsl (B) in
426 addition to zinc concentrations with plan sections at 120 mbsl (C) and 250 mbsl (D).

427
Corresponding author current address: Camborne School of Mines, University of Exeter, Penryn Campus, Cornwall, TR10 9FE

1
2
3
4
5
6
7
8
9
10
11
12
13
14
15
16
17
18
19
20
21
22
23
24
25
26
27
28
29
30
31
32
33
34
35
36
37
38
39
40
41
42
43
44
45
46
47
48
49
50
51
52
53
54
55
56
57
58
59
60
61
62
63
64
65

428 Fig. 5. Schematic summary of the relationship between diatremes, fluid flow and BMBs. A:
429 Late-stage magmatic intrusions within the diatremes and country rock. Hydrothermal fluids
430 utilize the diatremes, causing dolomitization during the waning stages of eruption. Fluids were
431 channeled into the fractured country rocks forming dissolution BMBs. B: Hydrothermal metal-
432 rich and brine-derived hydrothermal fluids utilized the porous diatreme fill. Note $\delta^{34}\text{S}$ values
433 shown are means for each category.

Figure 1 revised

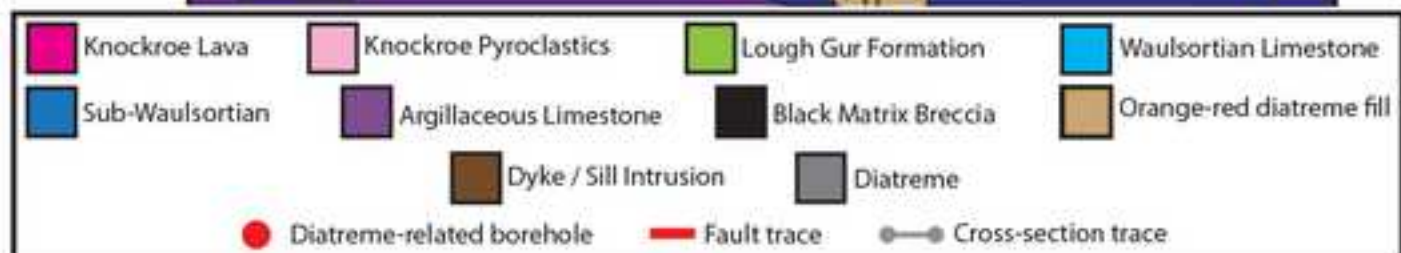
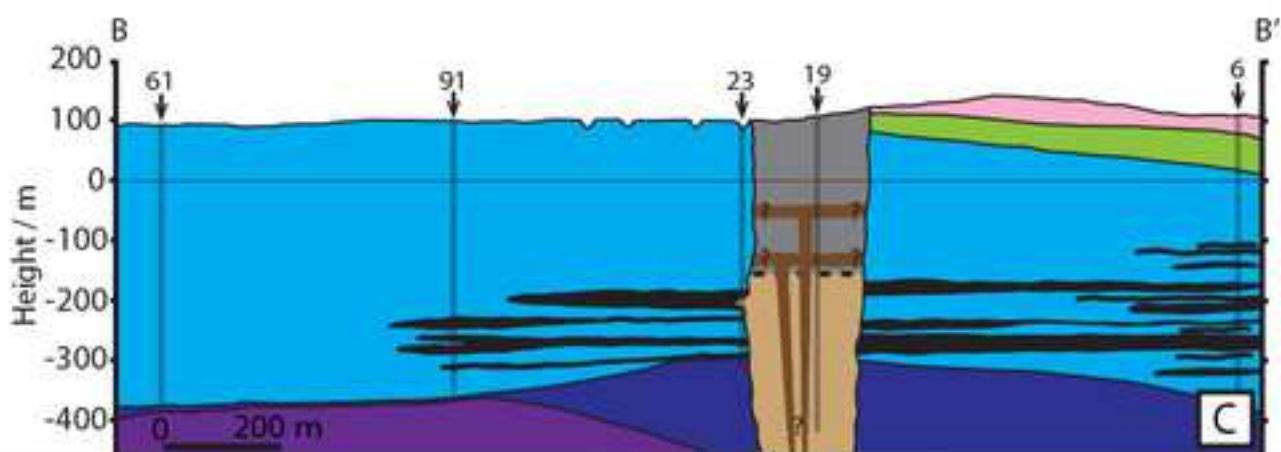
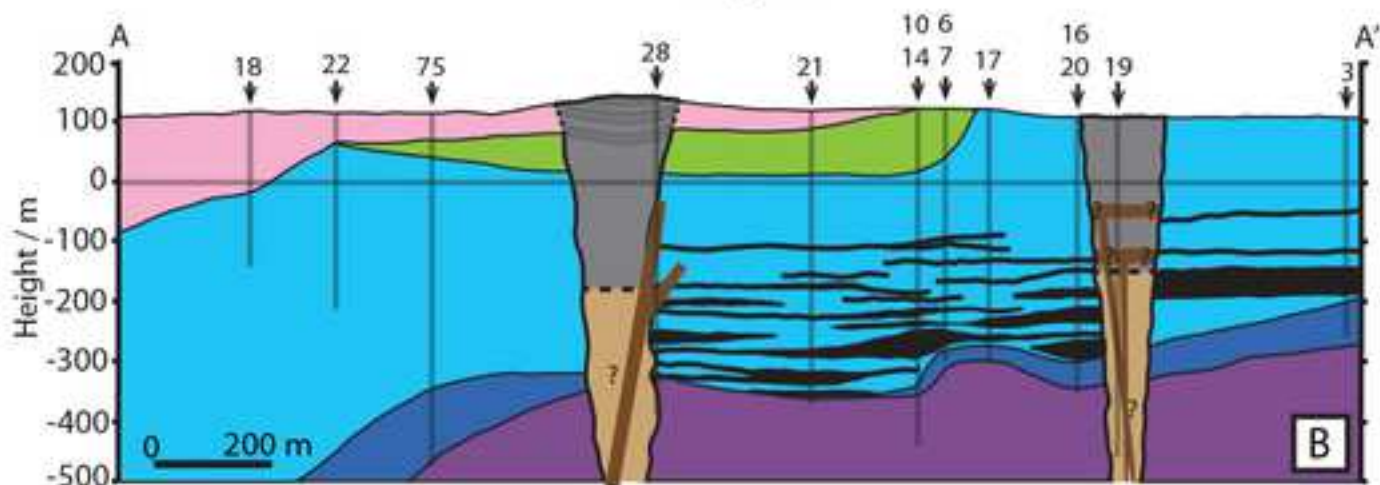
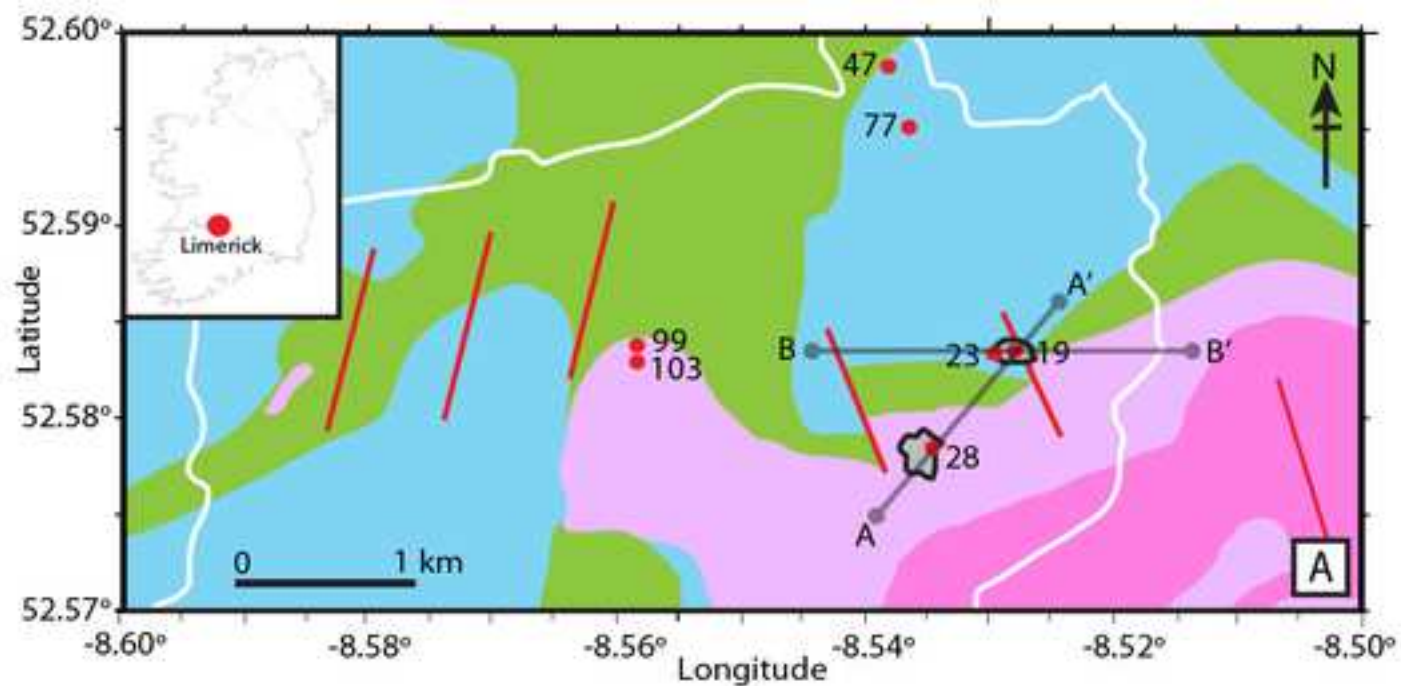


Figure 2

| A Stage: | Pre-ore volcanism | Pre-ore dolomitization | Pre-ore stage 1 | Pre-ore stage 2 | Ore stage | Post-ore stage |
|-----------------|--|------------------------|---------------------------|--------------------------|---|--------------------|
| Minerals: | Glassy lapilli + ash | Dol + Ap + It | Pyr ± Sph Disseminated | Pyr Layered/Colloform | Sph + Gal + Carb Replacement / Voids | Pyr Brecciating |
| Volcanic | [Grey shaded area indicating presence across stages] | | | | | |
| Limestone | [Grey shaded area indicating presence across stages] | | | | | |
| BMB Type R | [Grey shaded area indicating presence across stages] | | | | | |
| BMB Type P | [Grey shaded area indicating presence across stages] | | | | | |

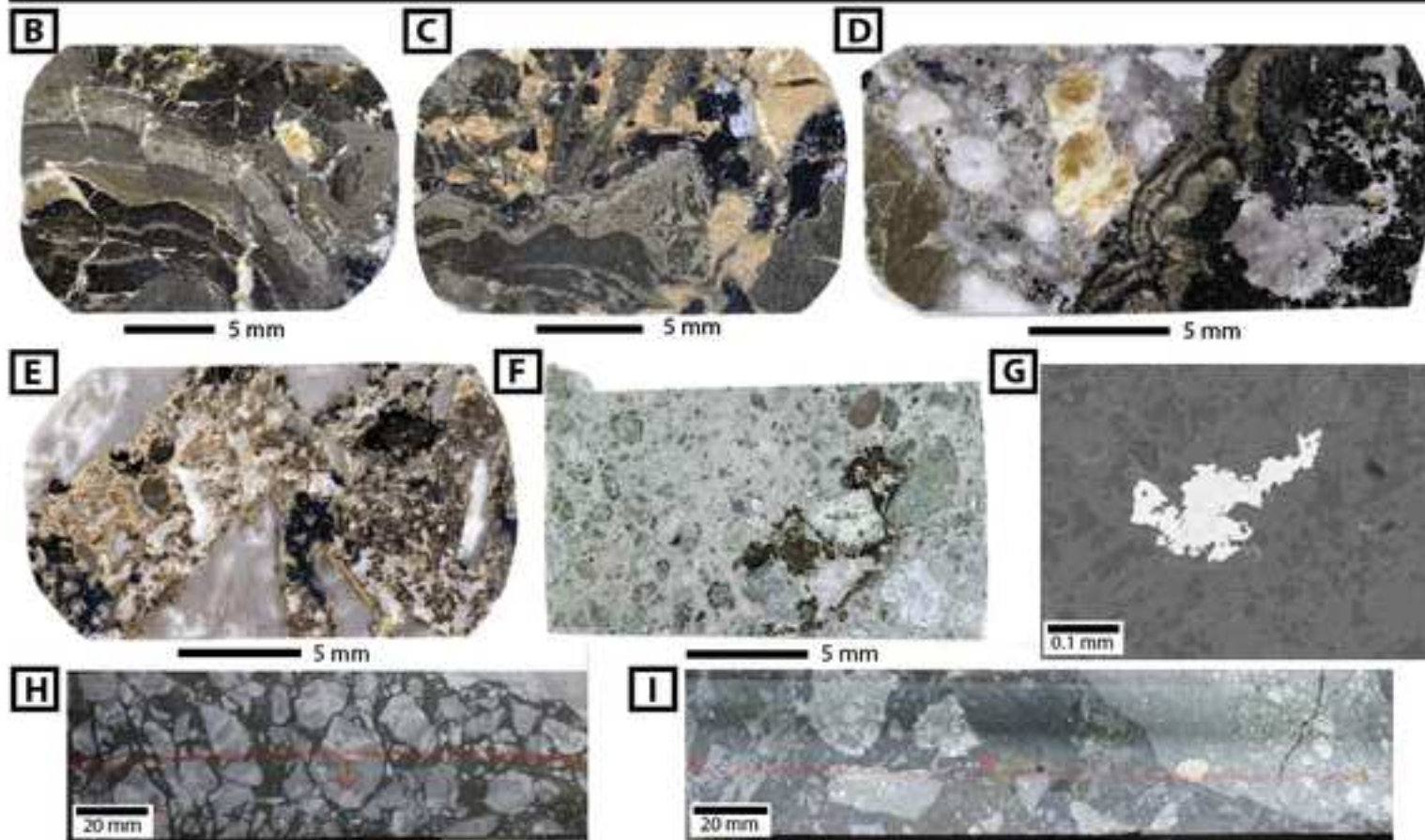


Figure 3

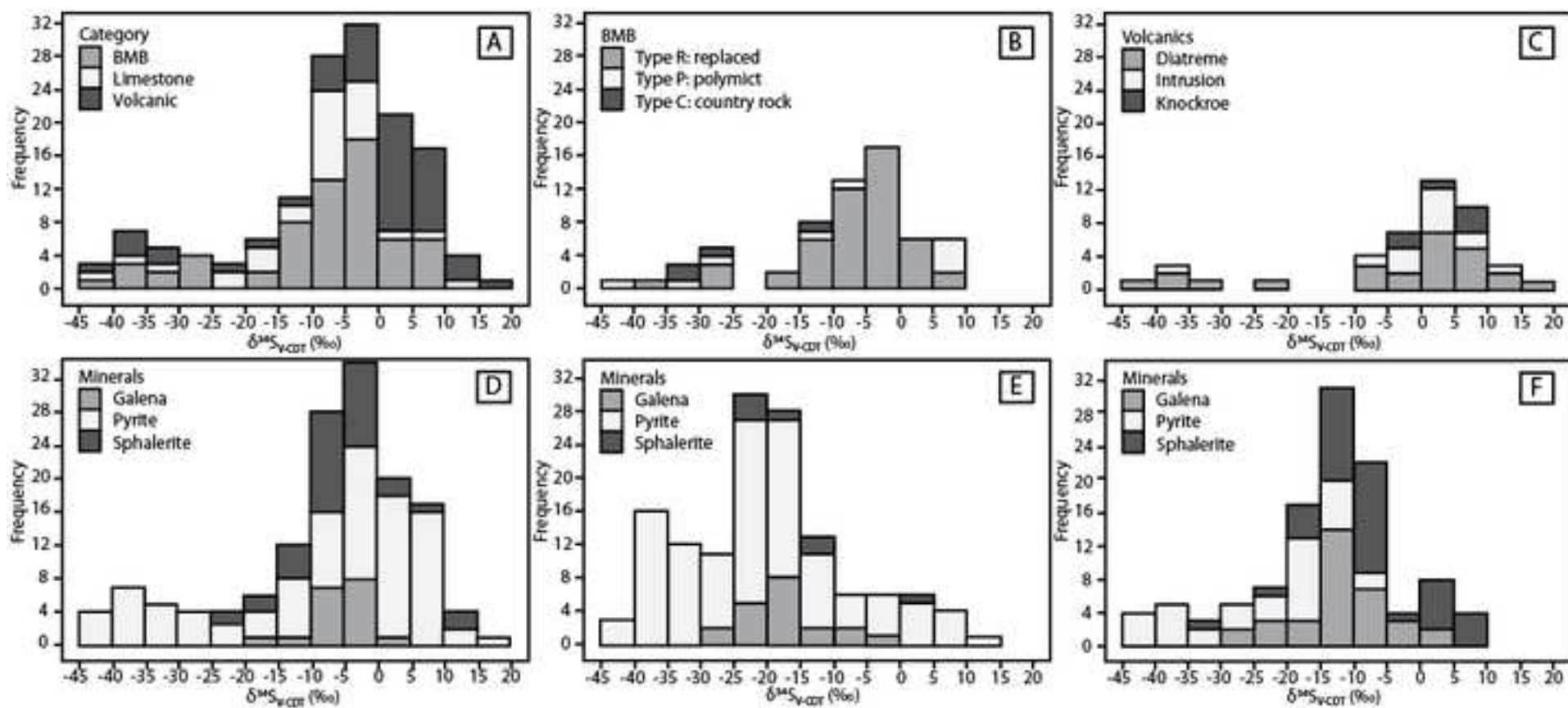


Figure 4

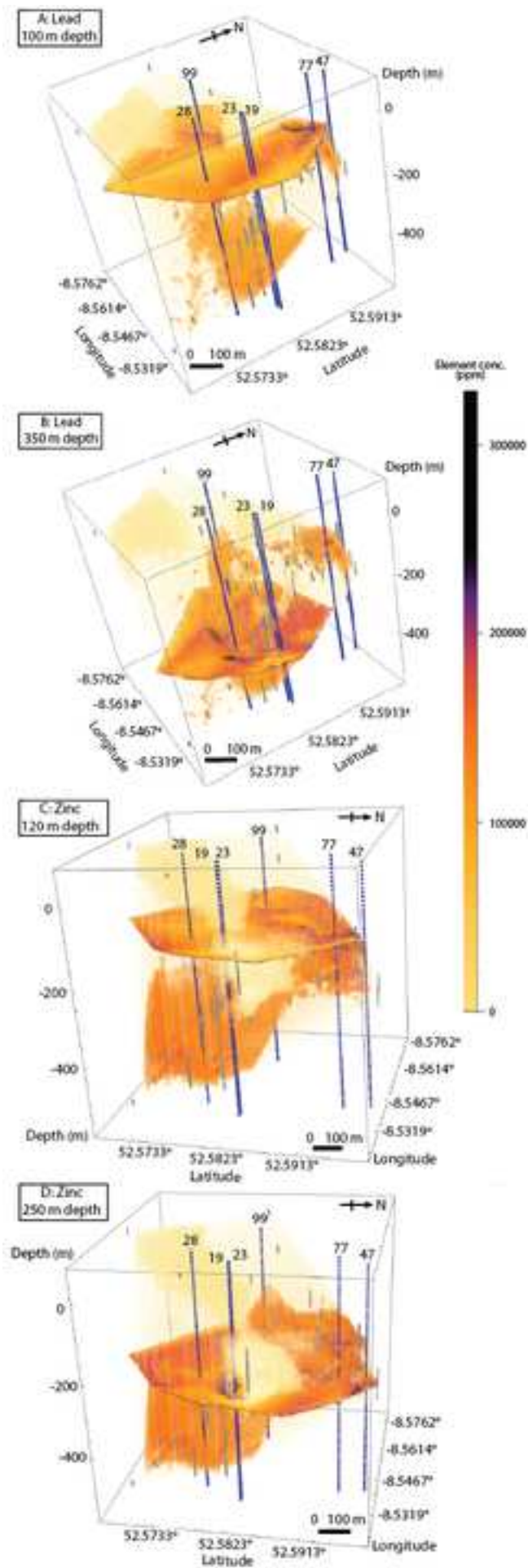


Figure 5 revised

